Supplementary Information

Monitoring intramolecular proton transfer with ion mobility-mass spectrometry and in-source ion activation

Younes Valadbeigi* and Tim Causon*

University of Natural Resources and Life Sciences, Vienna, Department of Chemistry, Institute of Analytical Chemistry, Muthgasse 18, 1190 Vienna, Austria

Emails: y.valadbeigi@boku.ac.at; tim.causon@boku.ac.at

Instrumentation

An Agilent 6560 IM-QTOF mass spectrometer was used for all measurements. A Dual Jetstream electrospray ion source (ESI) and a corona discharge atmospheric pressure chemical ionization (APCI) source (G1947B, Agilent Technologies) were used for ionisation of the compounds. The instrument was calibrated prior to measurements in the 2 GHz extended dynamic range mode using the standard Dual Jetstream ESI ion source and following the recommended tune procedure of the manufacturer. Temperature and flow rate of the drying gas in ESI were 225 °C and 13 L min^{-1}, respectively. Temperature of vaporiser and pressure of the nebuliser in APCI were 350°C and 30 psi, respectively. The drift tube was operated with a pressure of 3.94 Torr at 26–27.25 °C with high purity nitrogen as the drift gas (Linde Gas GmbH, Vienna). A trap release time of 150 µs, trap filling time of 10 ms and maximum arrival time of 60 ms were applied as standard settings for IM-MS measurements, while a trap filling time of 1.25 ms was used for acquisition with 4-bit multiplexing. The in-source ion activation before the IM drift tube was performed using a prototype in-source ion activation hardware between the capillary exit lens and capillary cap (fragmentor) [1]. The capillary exit lens voltage is maintained at about 360 V (same as high-pressure funnel entrance voltage) and the in-source ion activation is achieved by raising the fragmentor voltage to 600 V so that the maximum ion collision voltage is 240 V.

Ionization mechanism in the APCI ion source

For the APCI source H_3O^+ and NO^+ are the main reactant ions (RIs) which ionize analytes via protonation ($[M+H]^+$) and electron transfer ($M^{+\cdot}$), respectively [2]. As solvent competes with the analyte for ionization, relative abundances of $[M+H]^+$ and $M^{+\cdot}$ ions are influenced by solvents. In methanol and water solvents with low basicities, the analyte is ionized mainly by protonation and formation of [M+H]+. Acetonitrile produces a trimer with high basicity in the Agilent APCI ion source which depletes H_3O^+ RI to be protonated. Hence, in acetonitrile NO^+ can ionize analytes via electron transfer and formation of $M^{+\cdot}$ [2]. Further details can be found in [2].

Materials and method

1-Aminonaphthalene (99%), 2-aminonaphthalene (analytical standard), 1-aminoanthracene (90%), 2-aminoanthracene (96%), 9-aminophenanthrene (96%), and 1-aminopyrene (97%) were purchased from Sigma-Aldrich (Vienna, Austria). Methanol (99.9%), acetonitrile (99.9%), and formic acid (97.5%) were purchased from Honeywell. The concentration of polycyclic aromatic amines in all measurements was 10 µmol L^{-1}. A syringe pump (KD Scientific, Series 100, USA) was used to infuse solutions with flow rate of 20 µL min^{-1} into the nebuliser. A commercially available tune mix (ESI-L Low Concentration Tuning Mix, G1969-85000, Agilent Technologies) was prepared according to manufacturer instructions for tuning and accurate mass calibration of the mass spectrometer. Agilent IM-MS Browser 10.0 was used for single-field calibration and $^{DT}CCS_{N2}$ calculation. PNNL Preprocessor was used for demultiplexing and data pre-processing steps [3], Agilent Mass Profiler 10.0.2.202 was used for feature extraction, followed by high-resolution demultiplexing (HRdm) of the DTIM-MS data with Agilent HRdm 2.0 [4].

Computational details

Benchmark studies on the assessment of different methods of density functional theory (DFT) show that ωB97xD functional is one of the best functionals giving energetic values and structural parameters with reasonable precision [5,6]. Hence, ωB97xD was used for Structural optimization and energy calculation of all neutral and protonated PAAs. For additional comparison, the calculations in gas phase were performed using B3LYP. The relative energies calculated by ωB97xD and B3LYP for the protomers of PAAs are compared in Figures S1-S6 and show good agreement and predict the same relative stability trend for the protomers. The basis set 6-311++G(d,p) including diffuse and polarization functions for hydrogen and heavy atoms was used for the calculations. The transition state (TS) structures were obtained directly using opt=(ts,calcfc,noeigen) keywords followed by frequency calculations to prove the TS structure by its imaginary frequency. Further TS confirmation was done by intrinsic reaction coordinate (IRC) calculation. Proton affinity (PA) and gas phase basicity (GB) of the compounds were computed as $-\Delta H$ and $-\Delta G$ values of their protonation reactions in gas phase. Charge distribution calculation was carried using the Merz-Kollman (MK) method at the same level of theory. Tomasi's Polarized Continuum Model (PCM) was used for calculations in solvents water, methanol, and acetonitrile. Gaussian 16 software [7] was used for DFT calculations on the Vienna Scientific Cluster (VSC). The Gaussian output files containing geometric parameters of the optimized structures and MK charges were used to build input file for collision cross section (CCS) calculations. CCS calculations were performed on the VSC using MOBCAL-MPI software [8] using the trajectory method (TM) in nitrogen as buffer gas and at 298 K.

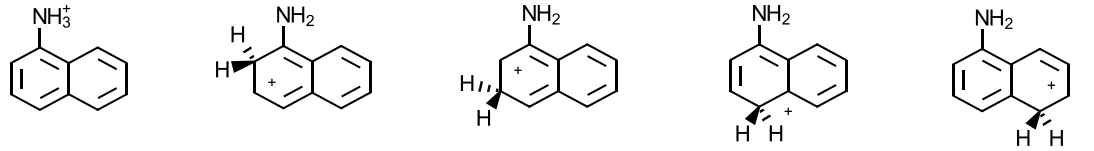

	1AN-a	1AN-b	1AN-c	1AN-d	1AN-e
Gas pahse	30.4 (31.1)	19.8 (18.8)	117.9 (106.2)	**0.0 (0.0)**	76.2 (69.1)
Acetonitrile	**0.0**	24.2	132.5	10.2	91.9
Methanol	**0.0**	24.1	132.2	9.9	91.7
Water	**0.0**	25.1	133.6	11.2	93.1

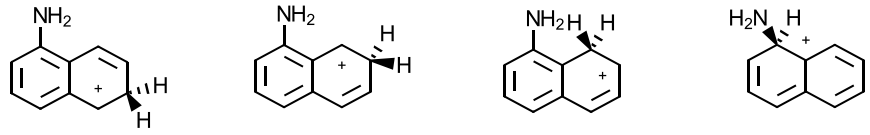

	1AN-f	1AN-g	1AN-h	1AN-i
Gas pahse	118.8 (105.9)	80.9 (72.2)	97.5 (88.3)	146.3 (140.7)
Acetonitrile	132.7	93.3	110.1	159.1
Methanol	132.5	93.1	109.9	158.9
Water	133.8	94.3	111.2	160.1

Figure S1. Comparison of ωB97XD-relative electronic energies of the protomers of 1-aminonaphthalene (1AN) in gas phase, acetonitrile, methanol, and water. The relative energies in parenthesis have been calculated by B3LYP for the protomers in gas phase. The energies are in kJ mol^{-1}.

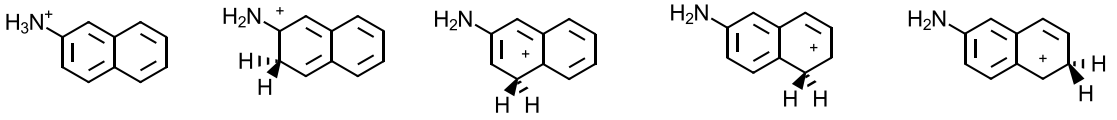

	2AN-a	2AN-b	2AN-c	2AN-d	2AN-e
Gas pahse	27.7 (28.9)	63.1(56.1)	101.6 (91.5)	90.4 (81.5)	42.6 (35.3)
Acetonitrile	**0.0**	83.4	122.4	114.3	69.5
Methanol	**0.0**	83.3	122.2	114.1	69.2
Water	**0.0**	84.6	123.6	115.6	70.8

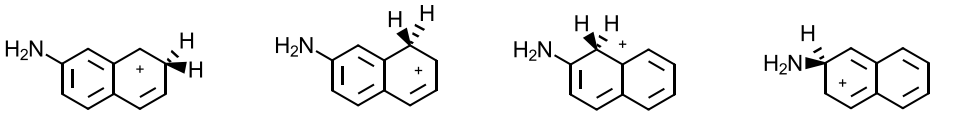

	2AN-f	2AN-g	2AN-h	2AN-i
Gas pahse	103.8 (92.4)	41.7 (34.4)	**0.0 (0.0)**	162.7 (157.8)
Acetonitrile	128.8	69.4	12.0	182.9
Methanol	128.5	69.2	11.8	182.7
Water	130.0	70.8	13.0	184.1

Figure S2. Comparison of ωB97XD-relative electronic energies of the protomers of 2-aminonaphthalene (2AN) in gas phase, acetonitrile, methanol, and water. The relative energies in parenthesis have been calculated by B3LYP for the protomers in gas phase. The energies are in kJ mol^{-1}.

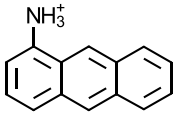

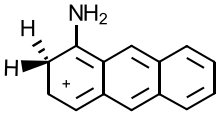

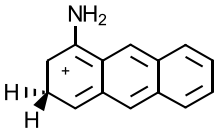

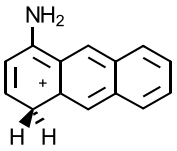

	1AA-a	1AA-b	1AA-c	1AA-d
Gas pahse	44.5 (44.6)	16.9 (15.1)	111.5 (98.7)	**0.0 (0.0)**
Acetonitrile	1.9	11.6	126.1	**0.0**
Methanol	2.1	11.6	121.6	**0.0**
Water	0.9	11.4	121.8	**0.0**

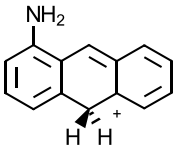

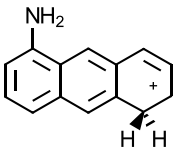

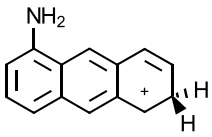

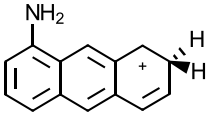

	1AA-e	1AA-f	1AA-g	1AA-h
Gas pahse	26.6 (23.7)	83.5 (68.5)	113.6 (98.8)	93.4 (78.5)
Acetonitrile	37.1	94.4	122.1	103.3
Methanol	37.1	94.3	122.1	103.2
Water	37.4	94.6	122.3	103.5

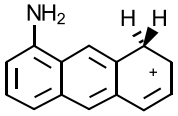

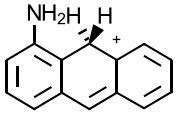

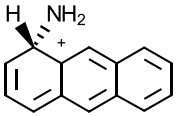

	1AA-i	1AA-j	1AA-k
Gas pahse	98.9 (86.6)	45.9 (40.7)	134.4 (125.1)
Acetonitrile	104.8	58.2	143.6
Methanol	104.8	58.2	143.5
Water	104.9	58.6	143.7

Figure S3. Comparison of ωB97XD-relative electronic energies of the protomers of 1-aminoanthracene (1AA) in the gas phase, acetonitrile, methanol, and water. The relative energies in parenthesis have been calculated by B3LYP for the protomers in the gas phase. The energies are in kJ mol^{-1}.

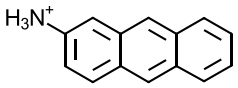

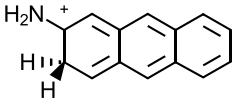

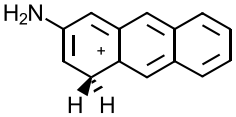

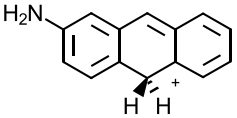

	2AA-a	2AA-b	2AA-c	2AA-d
Gas pahse	49.9 (53.3)	85.1 (77.1)	103.9 (94.6)	49.6 (47.6)
Acetonitrile	4.7	97.2	115.3	67.1
Methanol	4.8	97.1	115.2	67.0
Water	3.7	97.6	115.6	67.6

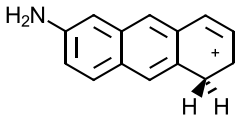

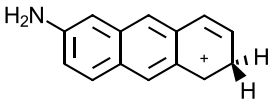

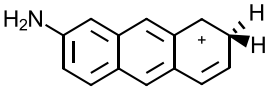

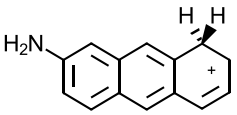

	2AA-e	2AA-f	2AA-g	2AA-h
Gas pahse	89.8 (82.4)	65.5 (55.8)	104.5 (94.4)	59.6 (49.9)
Acetonitrile	104.3	85.5	120.5	81.2
Methanol	104.2	85.4	120.4	81.1
Water	104.7	86.2	121.0	81.8

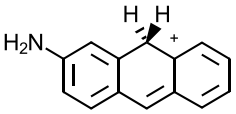

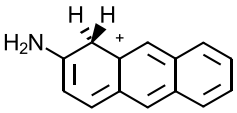

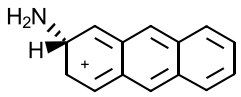

	2AA-i	2AA-j	2AA-k
Gas pahse	**0.0 (0.0)**	2.3 (3.9)	159.1 (154.3)
Acetonitrile	16.7	**0.0**	172.4
Methanol	16.6	**0.0**	172.3
Water	17.2	**0.0**	172.8

Figure S4. Comparison of ωB97XD-relative electronic energies of the protomers of 2-aminoanthracene (2AA) in the gas phase, acetonitrile, methanol, and water. The relative energies in parenthesis have been calculated by B3LYP for the protomers in gas phase. The energies are in kJ mol^{-1}.

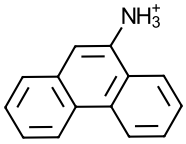

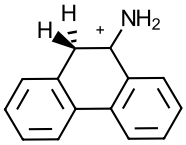

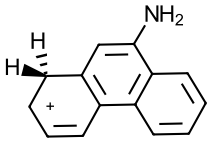

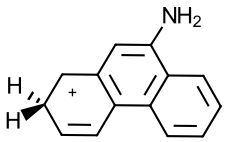

	9AP-a	9AP-b	9AP-c	9AP-d
Gas pahse	35.5 (33.3)	**0.0 (0.0)**	48.2 (36.7)	109.2 (91.6)
Acetonitrile	**0.0**	0.1	66.4	127.1
Methanol	0.1	**0.0**	66.3	127.0
Water	**0.0**	0.9	67.8	128.4

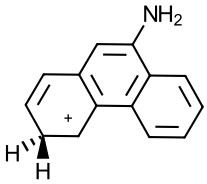

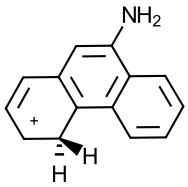

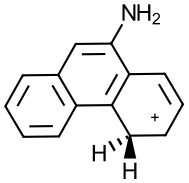

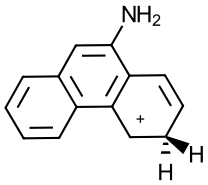

	9AP-e	9AP-f	9AP-g	9AP-h
Gas pahse	42.4 (31.3)	100.8 (86.2)	103.2 (90.5)	115.6 (96.7)
Acetonitrile	61.0	115.7	116.5	130.0
Methanol	60.9	115.6	116.4	129.9
Water	62.4	116.9	117.7	131.2

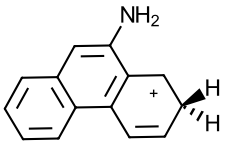

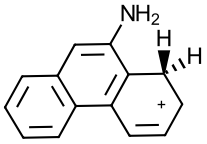

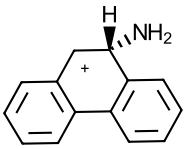

	9AP-i	9AP-j	9AP-k
Gas pahse	107.2 (90.9)	103.6 (86.1)	145.5 (135.1)
Acetonitrile	122.7	116.2	158.4
Methanol	122.7	116.1	158.3
Water	124.0	117.4	159.6

Figure S5. Comparison of ωB97XD-relative electronic energies of the protomers of 9-aminophenanthrene (9AP) in the gas phase, acetonitrile, methanol, and water. The relative energies in parenthesis have been calculated by B3LYP for the protomers in gas phase. The energies are in kJ mol^{-1}.

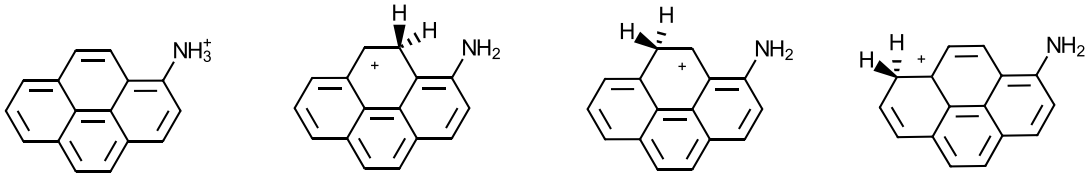

	1AP-a	1AP-b	1AP-c	1AP-d
Gas pahse	21.5 (28.8)	39.3 (40.7)	48.9 (45.8)	84.3 (80.6)
Acetonitrile	**0.0**	57.6	84.8	112.5
Methanol	**0.0**	57.4	84.5	112.3
Water	**0.0**	58.5	86.3	113.7

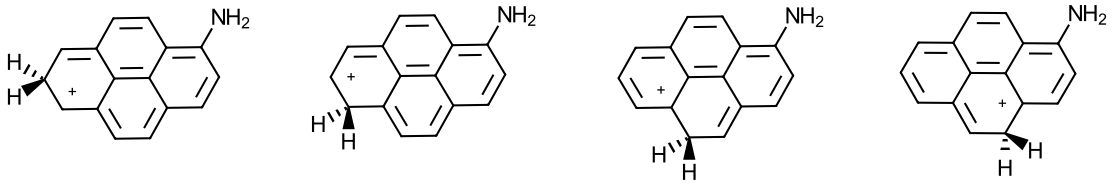

	1AP-e	1AP-f	1AP-g	1AP-h
Gas pahse	14.1 (17.9)	0.1 (0.9)	105.6 (95.8)	**0.0 (0.0)**
Acetonitrile	41.5	34.7	136.2	34.0
Methanol	41.3	34.5	136.0	33.7
Water	42.8	36.2	137.5	35.5

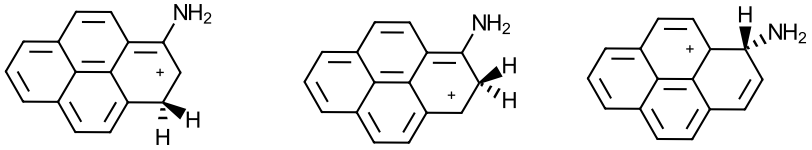

	1AP-i	1AP-j	1AP-k
Gas pahse	39.0 (44.2)	79.3 (78.6)	81.9 (82.5)
Acetonitrile	58.3	106.1	118.7
Methanol	58.1	105.9	118.4
Water	59.3	107.3	120.2

Figure S6. Comparison of ωB97XD-relative electronic energies of the protomers of 1-aminopyrene (1AP) in the gas phase, acetonitrile, methanol, and water. The relative energies in parenthesis have been calculated by B3LYP for the protomers in gas phase. The energies are in kJ mol^{-1}.

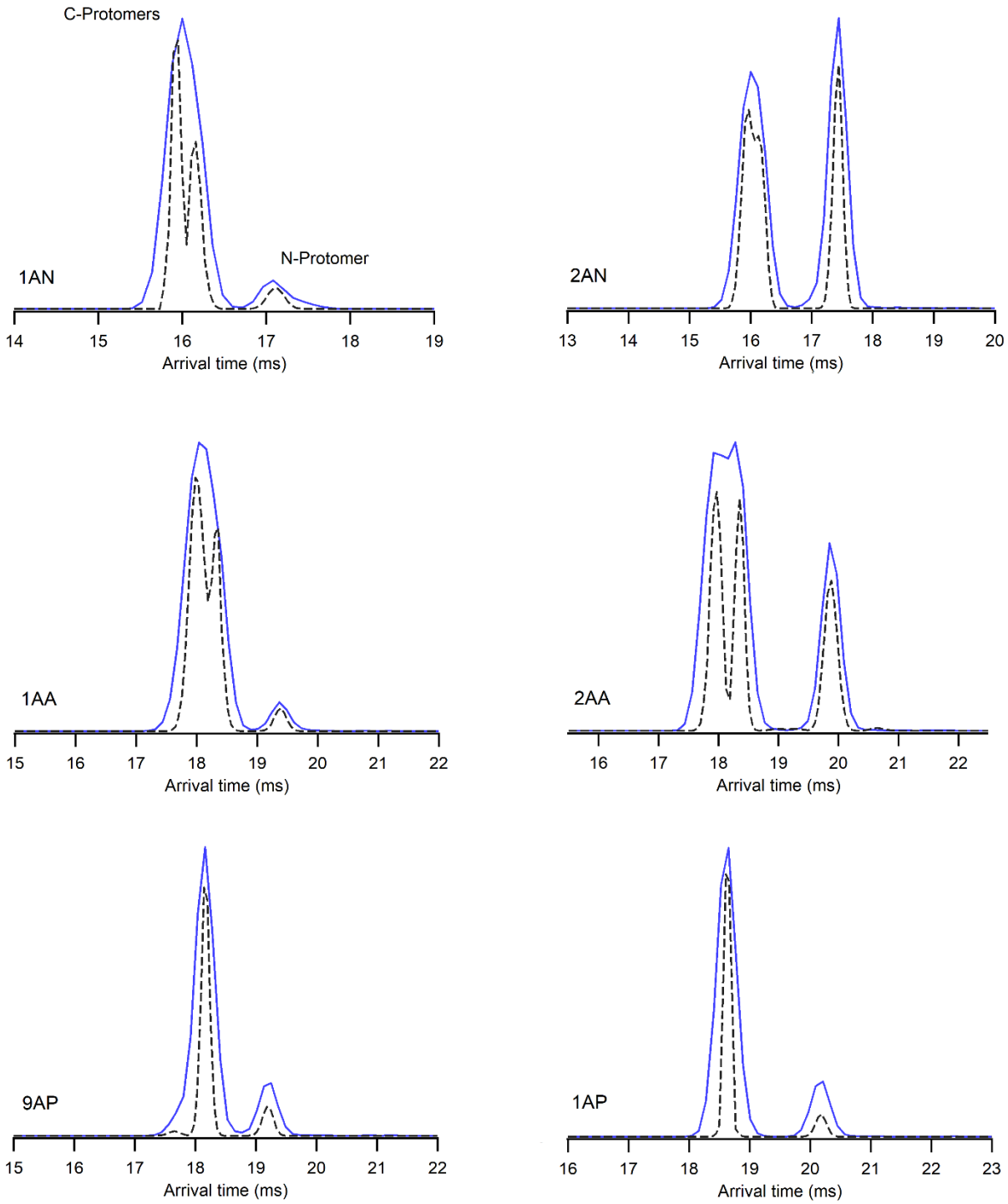

Figure S7. Comparison of standard (solid line) and HRdm (dashed line) IM spectra of $[M+H]^+$ ion of 1-aminonaphthalene (1-AN), 2-aminonaphthalene (2-AN), 1-aminoanthracene (1-AA), 2-aminoanthracene (2-AA), 9-aminophenanthrene (9-AP), and 1-aminopyrene (1-AP).

Table S1. Comparison of the experimental and calculated CCS_{N2} values of the C- and N-protomers of polycyclic aromatic amines (PAAs) and their dipole moments (μ_D). The CCS_{N2} and μ_D values are in Å^2 and Debye, respectively. For each PAA, CCS_{N2} and μ_D of the N-protomer are larger than those of the corresponding C-protomers. The "N" and "C" letters in parenthesis indicate the proton acceptor atom.

Protomer	μ_D (D)	CCS_{N2} (calculated)	$^{DT}CCS_{N2}$ (exp)
1AN-a (N)	8.00	134.2	135.5
1AN-b (C)	4.6	125.2	
1AN-c (C)	1.9	121.0	
1AN-d (C)	3.5	123.3	126.2
1AN-e (C)	1.8	123.3	
1AN-f (C)	2.0	121.7	
1AN-g (C)	3.4	123.3	
1AN-h (C)	2.3	122.5	
1AN-I (C)	2.6	120.7	
2AN-a (N)	10.7	137.2	138.3
2AN-b (C)	4.3	124.2	
2AN-c (C)	2.2	122.1	
2AN-d (C)	1.5	122.2	
2AN-e (C)	1.6	123.5	
2AN-f (C)	1.6	123.1	
2AN-g (C)	1.7	122.5	
2AN-h (C)	5.8	125.3	126.8
2AN-I (C)	0.6	121.2	
1AA-a (N)	10.1	147.9	150.4
1AA-b (C)	6.5	137.7	
1AA-c (C)	2.9	134.5	
1AA-d (C)	6.3	136.9	140.2
1AA-e (C)	2.8	134.9	
1AA-f (C)	3.2	133.9	
1AA-g (C)	3.4	135.2	
1AA-h (C)	3.9	134.9	
1AA-I (C)	4.5	135.8	
1AA-j (C)	0.8	133.9	
1AA-k (C)	4.0	134.7	
2AA-a (N)	14.3	153.0	154.3
2AA-b (C)	5.6	136.8	
2AA-c (C)	4.2	135.2	
2AA-d (C)	0.9	134.0	
2AA-e (C)	3.3	136.4	
2AA-f (C)	1.6	136.1	
2AA-g (C)	2.6	135.7	
2AA-h (C)	0.6	134.9	
2AA-i (C)	4.3	135.7	
2AA-j (C)	8.8	139.3	140.2
2AA-k (C)	1.2	136.3	
9AP-a (N)	9.5	146.5	149.3
9AP-b (C)	6.1	137.0	141.0
9AP-c (C)	3.1	133.4	
9AP-d (C)	3.5	133.7	
9AP-e (C)	1.9	134.4	
9AP-f (C)	3.3	132.0	
9AP-g (C)	3.9	133.2	
9AP-h (C)	3.3	133.0	
9AP-I (C)	4.3	132.6	
9AP-j (C)	4.0	132.8	
9AP-k (C)	3.7	132.4	
1AP-a (N)	11.1	150.7	155.6
1AP-b (C)	7.0	141.1	
1AP-c (C)	1.1	136.2	
1AP-d (C)	3.1	137.8	
1AP-e (C)	4.8	139.1	
1AP-f (C)	2.6	138.9	
1AP-g (C)	3.2	138.0	
1AP-h (C)	3.4	138.6	143.6
1AP-I (C)	6.9	141.0	
1AP-j (C)	3.8	137.4	
1AP-k (C)	0.9	136.8	

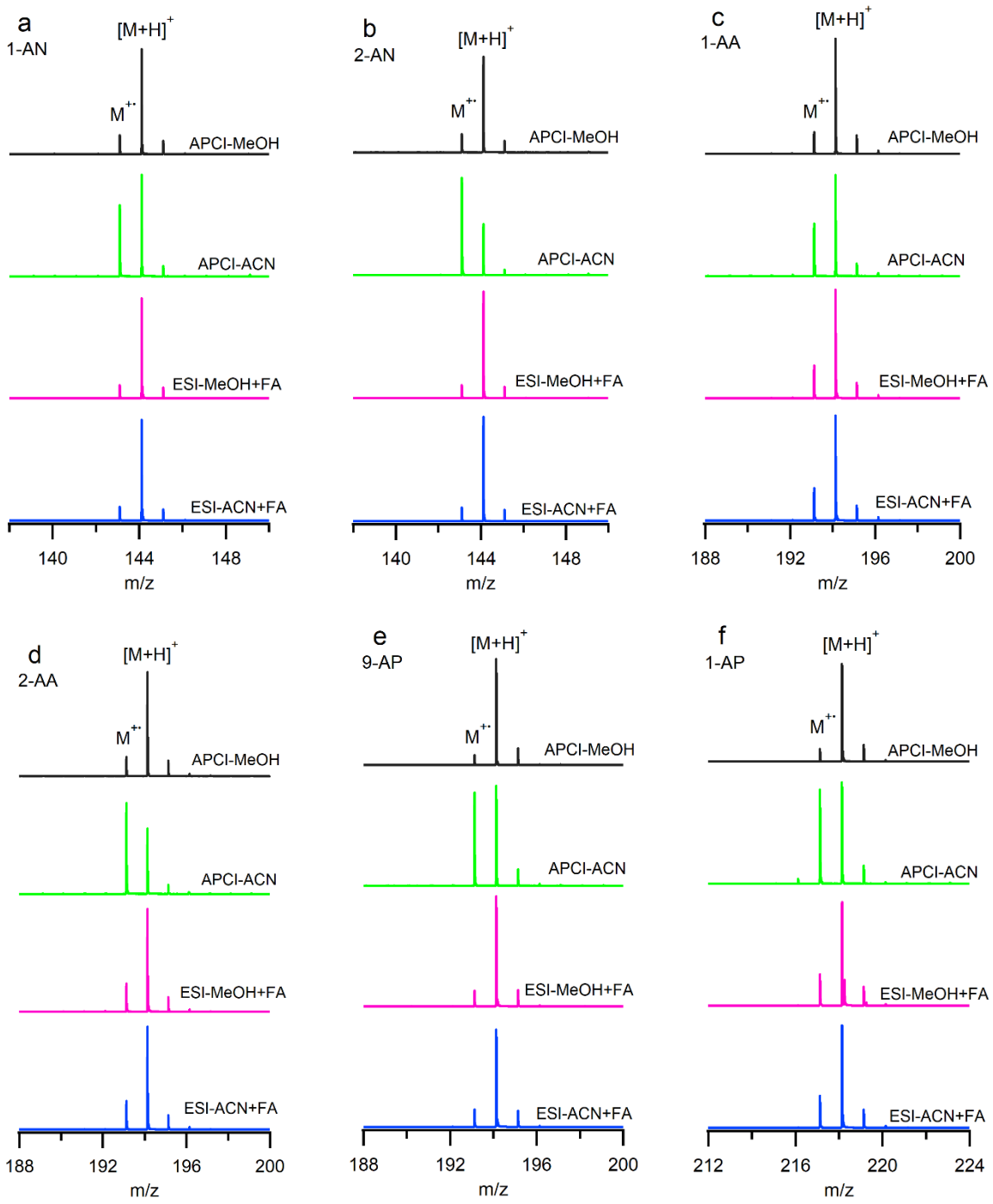

Figure S8. Comparison of mass spectra of (a) 1-aminonaphthalene (1-AN), (b) 2-aminonaphthalene (2-AN), (c) 1-aminoanthracene (1-AA), (d) 2-aminoanthracene (2-AA), (e) 9-aminophenanthrene (9-AP), and (f) 1-aminopyrene (1-AP) in ESI and APCI ion sources in acetonitrile (ACN) and methanol (MeOH) solvents. Standards were prepared in 0.01% (v/v) formic acid (FA) for ESI measurements.

Table S2. Calculated proton affinity (PA) and gas phase basicity (GB) for nitrogen and carbon atoms of the PAAs at 298 K. Only the PA and GB of the most basic carbon are shown.

	Nitrogen atom		Carbon atom	
Compound	PA (kJ mol^{-1})	GB (kJ mol^{-1})	PA (kJ mol^{-1})	GB (kJ mol^{-1})
1-Aminonaphthalene	899.7	868.9	935.7	906.5
2-Aminonaphthalene	897.0	867.6	927.7	901.6
1-Aminoanthracene	906.4	875.6	955.8	926.9
2-Aminoanthracene	902.6	872.6	954.8	926.7
9-Aminophenanthrene	905.5	874.9	945.3	914.8
1-Aminopyrene	909.4	878.5	937.7	908.6

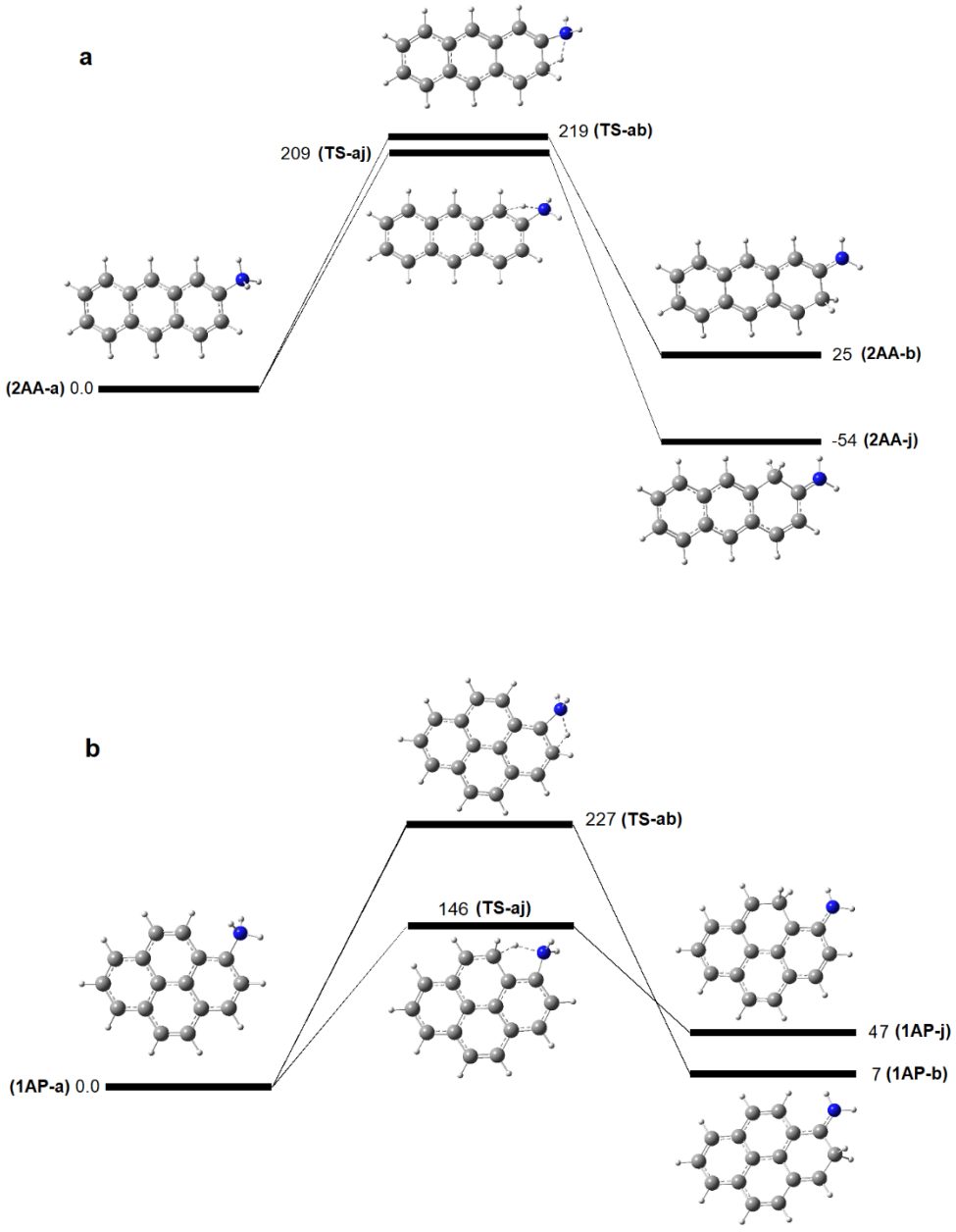

Figure S9. The optimized transition state (TS) structures and activation Gibbs free energies for intramolecular N→C proton transfer in (a) 2-aminoanthracene (2AA) and (b) 1-aminopyrene (1AP). The energies are in kJ mol^{-1}.

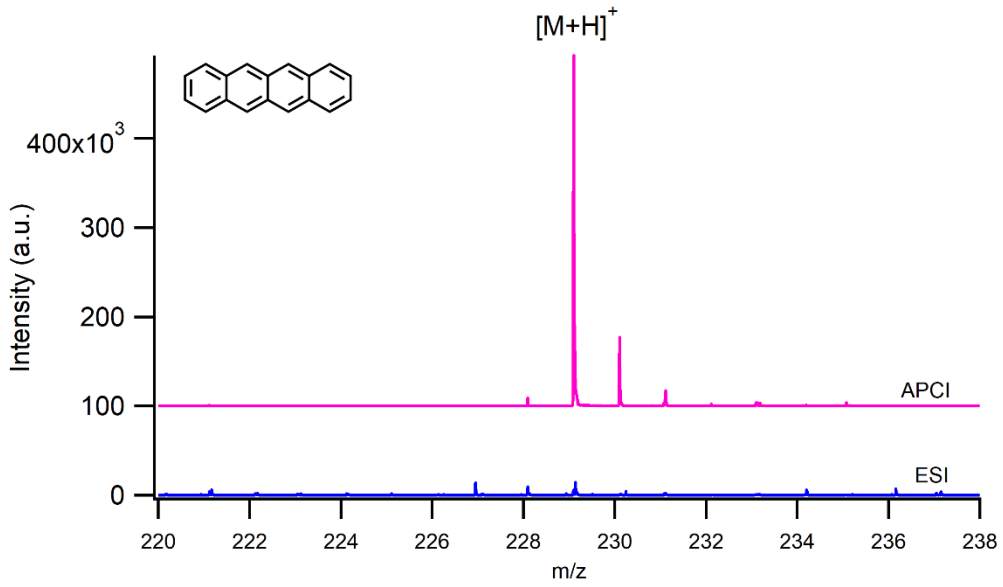

Figure S10. Comparison of mass spectra of tetracene ionised using: APCI (10 µmol L^{-1} in methanol) and ESI (10 µmol L^{-1} in methanol with 0.01% (v/v) formic acid). In ESI without formic acid, the intensity of the $[M+H]^+$ peak was even weaker. Hence, carbon atoms of the polycyclic aromatic rings are not protonated in solvent.

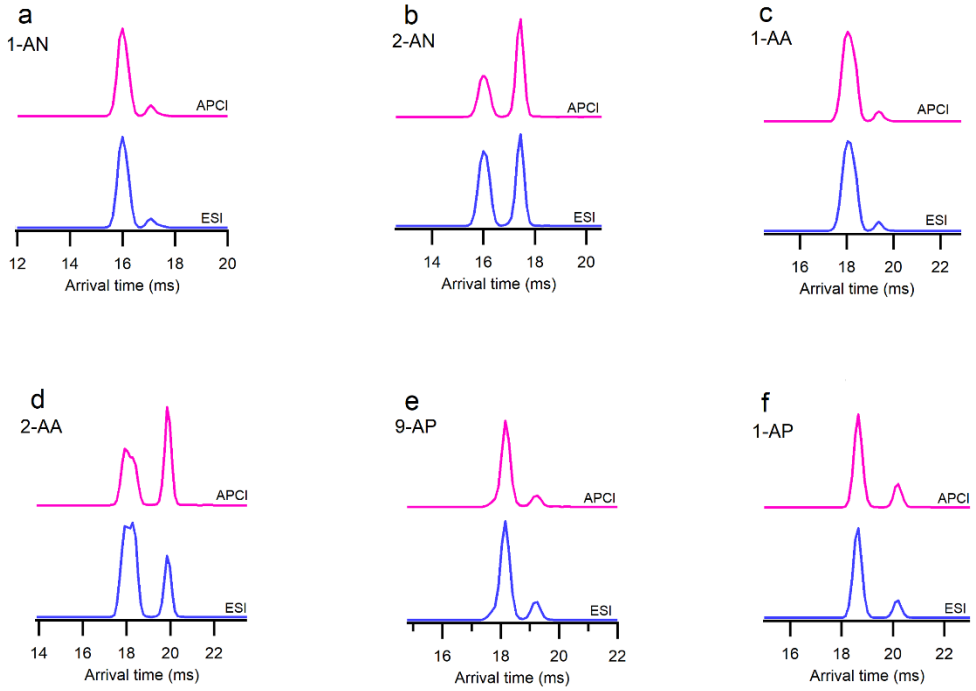

Figure S11. Comparison of IM-spectra of C- and N-protomers of (a) 1-aminonaphthalene (1-AN), (b) 2-aminonaphthalene (2-AN), (c) 1-aminoanthracene (1-AA), (d) 2-aminoanthracene (2-AA), (e) 9-aminophenanthrene (9-AP), and (f) 1-aminopyrene (1-AP) produced by APCI and ESI ion sources in methanol. No formic acid was added to solvent for ionisation in ESI.

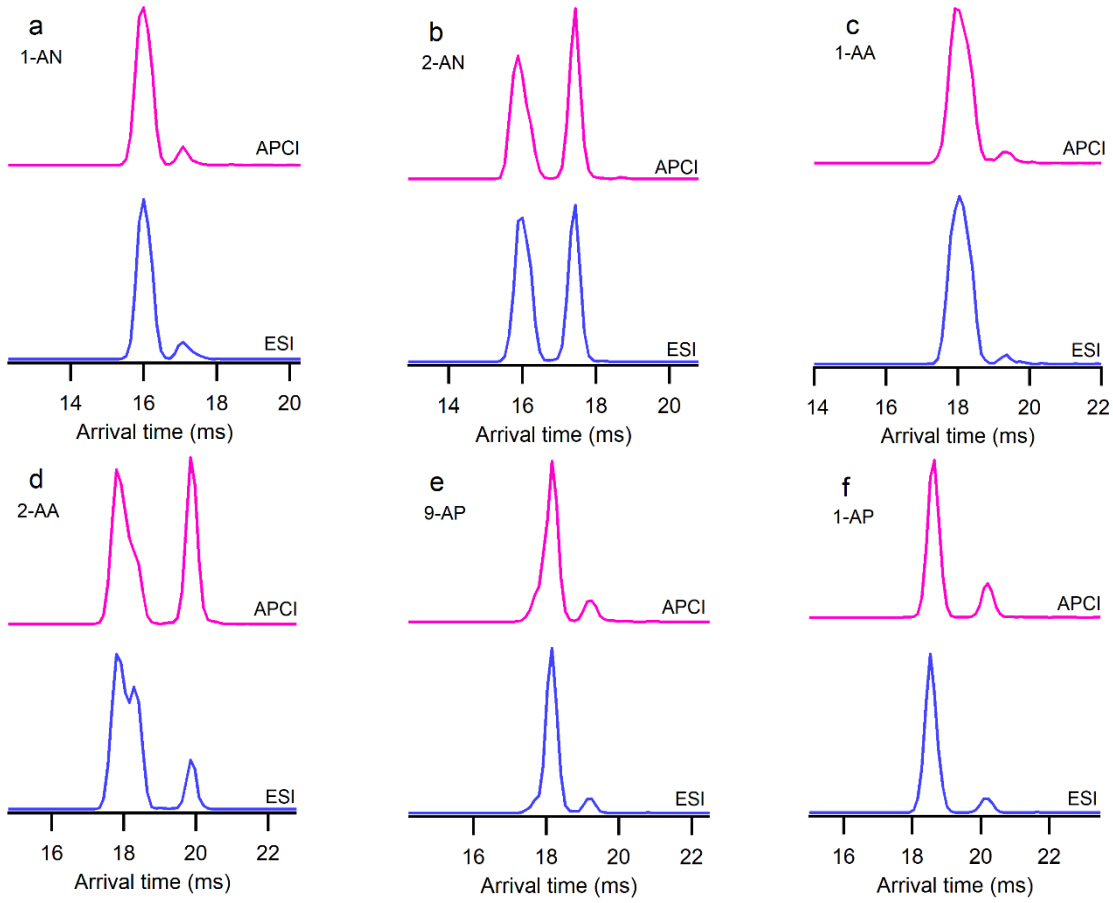

Figure S12. Comparison of IM-spectra of C- and N-protomers of (a) 1-aminonaphthalene (1-AN), (b) 2-aminonaphthalene (2-AN), (c) 1-aminoanthracene (1-AA), (d) 2-aminoanthracene (2-AA), (e) 9-aminophenanthrene (9-AP), and (f) 1-aminopyrene (1-AP) produced by APCI and ESI ion sources in acetonitrile. No formic acid was added to solvent for ionization in ESI.

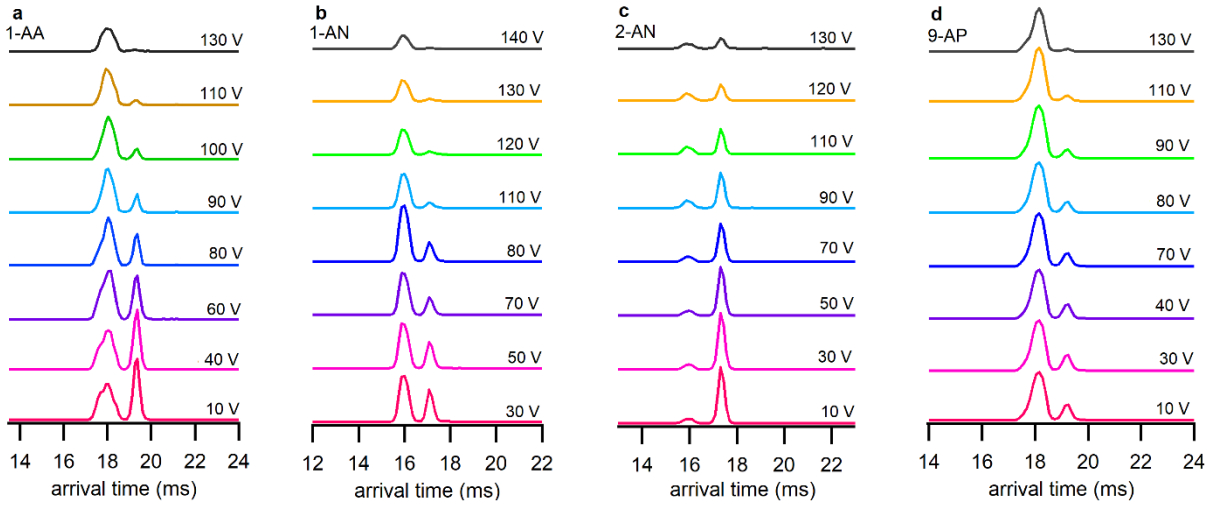

Figure S13. Effect of in-source ion activation (collision voltages) on the relative intensities of N- and C-protomers of (a) 1-aminoanthracene (1-AA), (b) 1-aminonaphthalene(1-AN), (c) 2-aminonaphthalene (2-AN), and (d) 9-aminophenanthrene (9-AP).

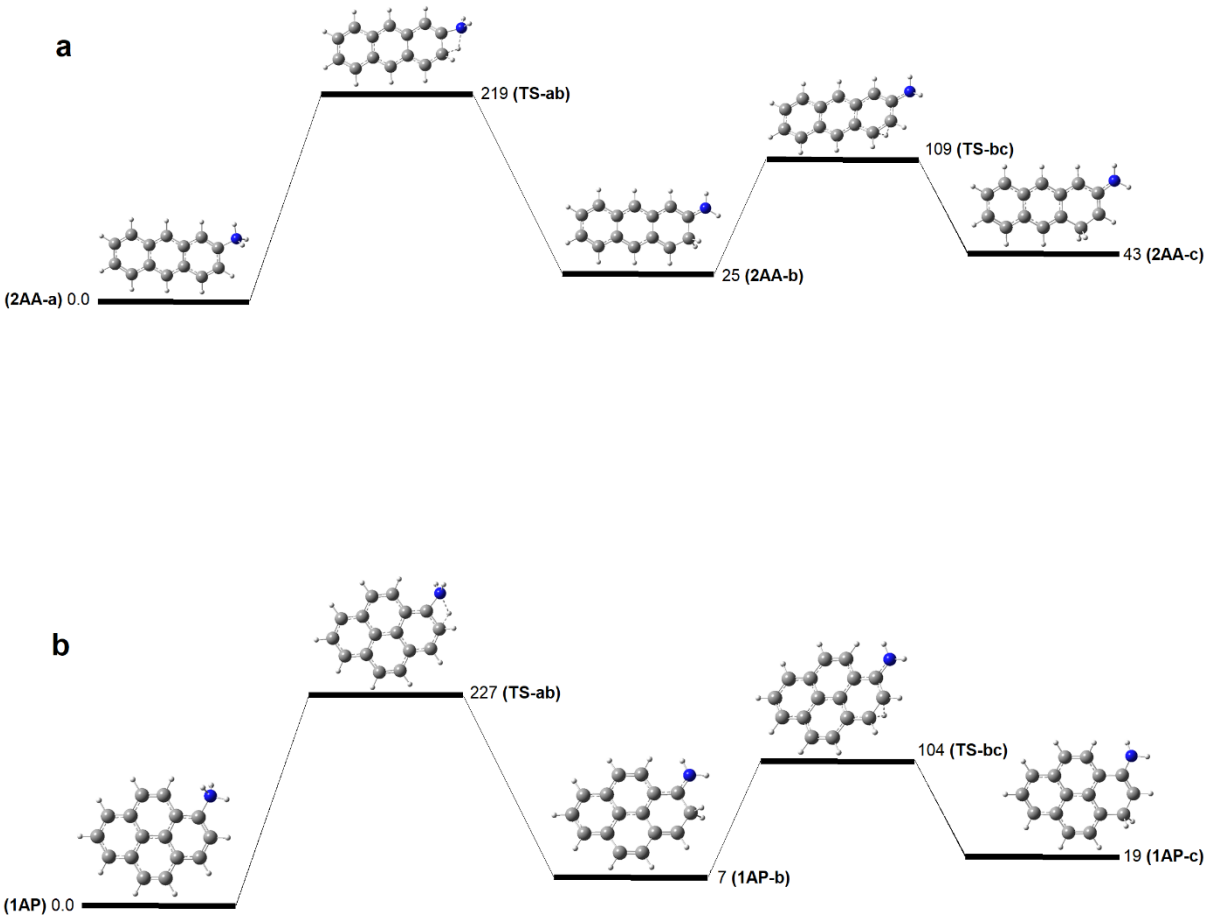

Figure S14. The optimized transition state (TS) structures and activation Gibbs free energies for intramolecular N→C and C→C proton transfer in (a) 2-aminoanthracene (2AA) and (b) 1-aminopyrene (1AP). The energies are in kJ mol^{-1}.

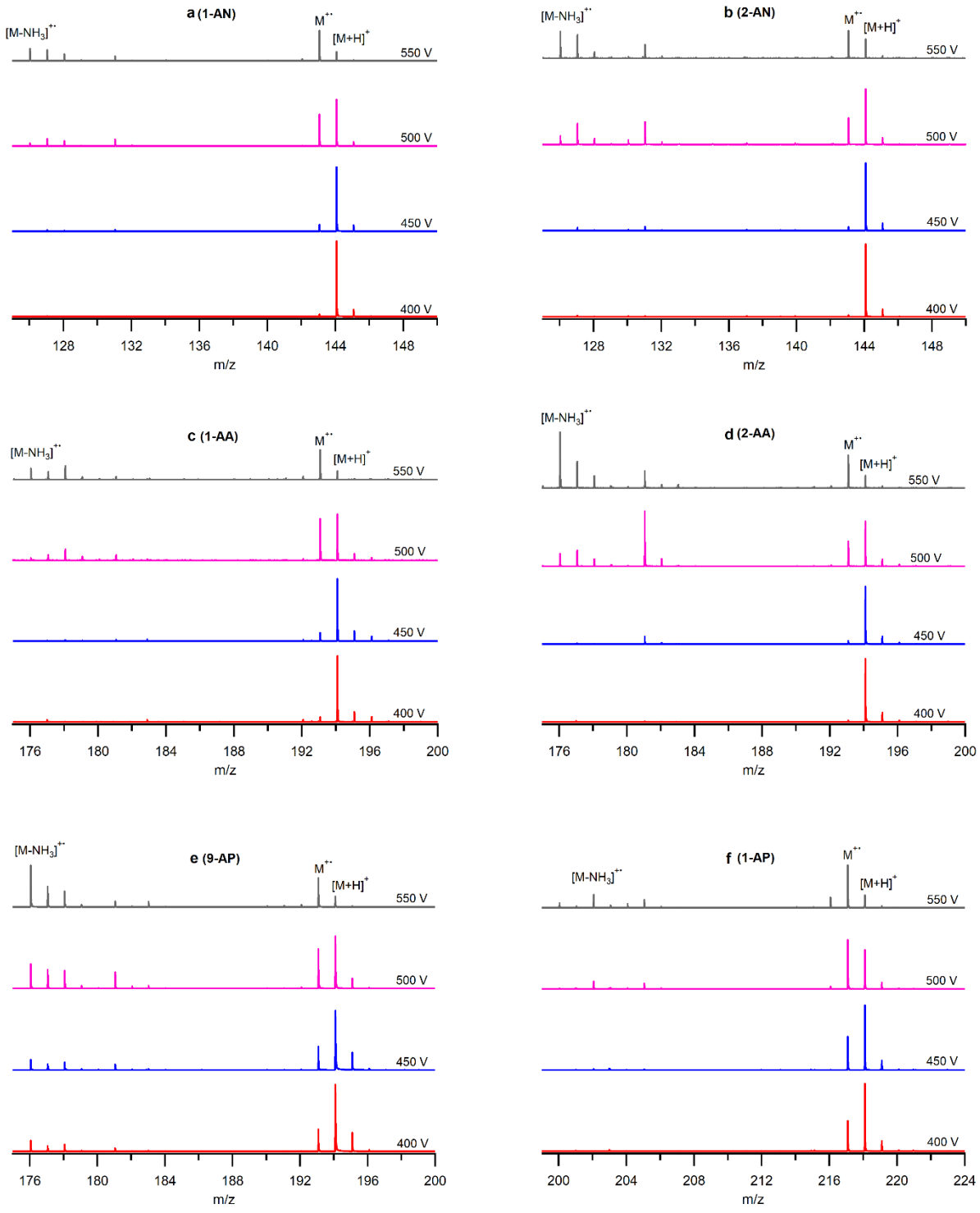

Figure S15. ESI-mass spectra of (a) 1-aminonaphthalene (1-AN), (b) 2-aminonaphthalene (2-AN), (c) 1-aminoanthracene (1-AA), (d) 2-aminoanthracene (2-AA), (e) 9-aminophenanthrene (9-AP), and (f) 1-aminopyrene (1-AP) using different in-source collision voltages (concentration: 10 µmol L^{-1} in 1:1 (v/v) CH_3OH:H_2O with 0.01% (v/v) formic acid).

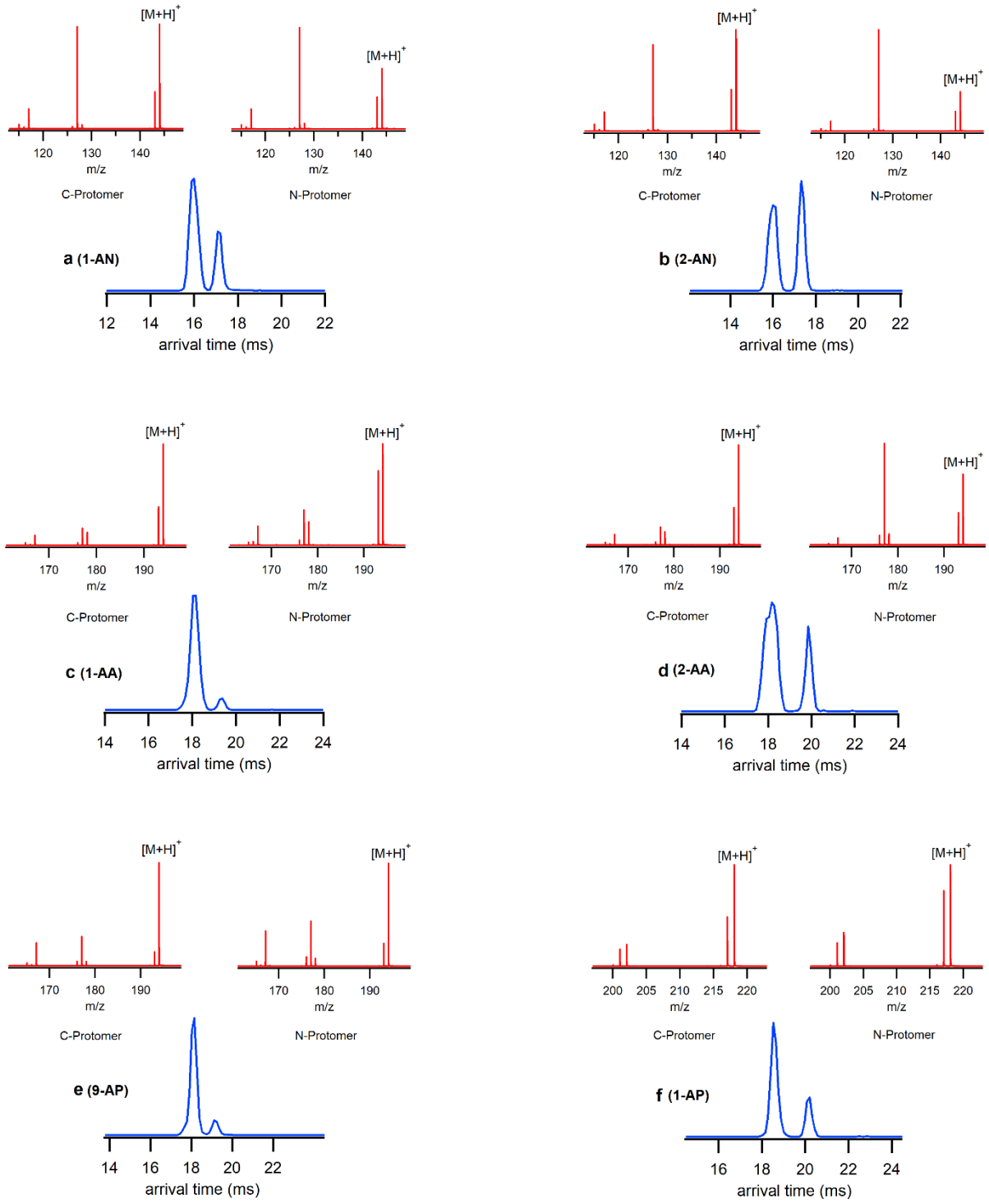

Figure S16. Comparison of HR-MS fragment spectra of C- and N-protomers of (a) 1-aminonaphthalene (1-AN), (b) 2-aminonaphthalene (2-AN), (c) 1-aminoanthracene (1-AA), (d) 2-aminoanthracene (2-AA), (e) 9-aminophenanthrene (9-AP), and (f) 1-aminopyrene (1-AP) with CID voltage of 15 V. (10 µmol L^{-1} in 1:1 (v/v) H_2O:CH_3OH). Mass spectra are normalised to the most intense peak in the spectrum.

References

1. X. Zheng, R. T. Kurulugama, A. Laganowsky, D. H. Russell, Collision-induced unfolding studies of proteins and protein complexes using drift tube ion mobility-mass spectrometer. *Anal. Chem*. 2020, **92**, 7218-7225.

2. Y. Valadbeigi and T. Causon, Significance of Competitive Reactions in an Atmospheric Pressure Chemical Ionization Ion Source: Effect of Solvent. *J. Am. Soc. Mass Spectrom*. 2022, **33**, 961-973.

3. A. Bilbao, B. C. Gibbons, S. M. Stow, J. E. Kyle, K. J. Bloodsworth, S. H. Payne, R. D. Smith, Y. M. Ibrahim, E. S. Baker, J. C. Fjeldsted, A preprocessing tool for enhanced ion mobility–mass spectrometry-based omics workflows. *J. Proteome Res*. 2022, **21**, 798–807.

4. J. C. May, R. Knochenmuss, J. C. Fjeldsted, J. A. McLean, Resolution of isomeric mixtures in ion mobility using a combined demultiplexing and peak deconvolution technique. *Anal. Chem*. 2020, **92**, 9482-9492.

5. G. F. Mangiatordi, E. Brémond, C. Adamo, DFT and Proton Transfer Reactions: A Benchmark Study on Structure and Kinetics. *J. Chem. Theory Comput*. 2012, **8**, 3082–3088.

6. K. S. Thanthiriwatte, E. G. Hohenstein, L. A. Burns, C. D. Sherrill, Assessment of the Performance of DFT and DFT-D Methods for Describing Distance Dependence of Hydrogen-Bonded Interactions. J. *Chem. Theory Comput*. 2011, **7**, 88–96

7. Gaussian 16, Revision C.01, M. J. Frisch, G. W. Trucks, H. B. Schlegel, G. E. Scuseria, M. A. Robb, J. R. Cheeseman, G. Scalmani, V. Barone, G. A. Petersson, H. Nakatsuji, X. Li, M. Caricato, A. V. Marenich, J. Bloino, B. G. Janesko, R. Gomperts, B. Mennucci, H. P. Hratchian, J. V. Ortiz, A. F. Izmaylov, J. L. Sonnenberg, D. Williams-Young, F. Ding, F. Lipparini, F. Egidi, J. Goings, B. Peng, A. Petrone, T. Henderson, D. Ranasinghe, V. G. Zakrzewski, J. Gao, N. Rega, G. Zheng, W. Liang, M. Hada, M. Ehara, K. Toyota, R. Fukuda, J. Hasegawa, M. Ishida, T. Nakajima, Y. Honda, O. Kitao, H. Nakai, T. Vreven, K. Throssell, J. A. Montgomery, Jr., J. E. Peralta, F. Ogliaro, M. J. Bearpark, J. J. Heyd, E. N. Brothers, K. N. Kudin, V. N. Staroverov, T. A. Keith, R. Kobayashi, J. Normand, K. Raghavachari, A. P. Rendell, J. C. Burant, S. S. Iyengar, J. Tomasi, M. Cossi, J. M. Millam, M. Klene, C. Adamo, R. Cammi, J. W. Ochterski, R. L. Martin, K. Morokuma, O. Farkas, J. B. Foresman, and D. J. Fox, Gaussian, Inc., Wallingford CT, 2016.

8. C. Ieritano, J. Crouse, J. L. Campbell, W. S. Hopkins, A parallelized molecular collision cross section package with optimized accuracy and efficiency. *Analyst*, 2019,**144**, 1660-1670.